IOPscience iopscience.iop.org

Home Search Collections Journals About Contact us My IOPscience

Polar and nonpolar GaN quantum dots

This article has been downloaded from IOPscience. Please scroll down to see the full text article.

2008 J. Phys.: Condens. Matter 20 473201

(http://iopscience.iop.org/0953-8984/20/47/473201)

View the table of contents for this issue, or go to the journal homepage for more

Download details:
IP Address: 129.252.86.83
The article was downloaded on 29/05/2010 at 16:39

Please note that terms and conditions apply.

IOP Publishing Journal of Physics: Condensed Matter
J. Phys.: Condens. Matter **20** (2008) 473201 (15pp) doi:10.1088/0953-8984/20/47/473201

TOPICAL REVIEW

Polar and nonpolar GaN quantum dots

Bruno Daudin

CEA-CNRS group 'Nanophysique et Semiconducteurs', CEA Grenoble, INAC/SP2M, 17 rue des Martyrs, 38 054 Grenoble, France

Received 23 April 2008, in final form 5 August 2008
Published 6 November 2008
Online at stacks.iop.org/JPhysCM/20/473201

Abstract
Growth, structural and optical properties of GaN quantum dots are reviewed, with a special emphasis on plasma-assisted molecular beam epitaxy. The versatility of this technique makes it particularly adapted to growth of quantum dots, either polar (c-plane) or nonpolar (a-plane and m-plane). After describing in detail the growth process and analyzing the morphology of the dots, we review the optical properties of these nanostructures and discuss the properties of single dots.

(Some figures in this article are in colour only in the electronic version)

Contents

1. Introduction 1
2. Epitaxial growth of nitrides 2
   2.1. Generalities 2
   2.2. GaN growth kinetics 2
3. Growth of GaN QDs 3
   3.1. Structural properties of GaN QDs 4
4. Capping and vertical correlation of GaN QDs 5
   4.1. Capping phenomenology 5
   4.2. Vertical correlation of stacked QDs 7
5. Optical properties 9
   5.1. Emission of an ensemble of GaN QDs 9
   5.2. Emission of polar single QDs 11
   5.3. Emission of nonpolar single QDs 12
6. Conclusion 13
Acknowledgments 13
References 13

1. Introduction

It has now become almost unnecessary to justify the huge interest in wide bandgap nitride semiconductors, namely InN, GaN and AlN. As a matter of fact, due to the extended range of their bandgap energy value (∼0.7 eV for InN, ∼3.5 eV for GaN, ∼6.2 eV for AlN) these binary semiconductors and their ternary or quaternary alloys present a widely recognized potential for light emission/detection in a wavelength range spanning from infrared (IR) to ultraviolet (UV).

On the other hand, there is no further need to justify the interest in QDs from both fundamental and applied point of view. Besides the well known consequences of three-dimensional (3D) quantization, which provides new degrees of freedom for the design of advanced devices allowing one for instance to tailor emission/absorption energy, one practical aspect of QDs is related to their relative insensitivity to the structural defects in the surrounding matrix. In other words, QDs can be considered as perfect objects in a defective matrix. This remarkable property is of particular interest in the case of nitride materials. As a matter of fact, the persisting lack of low-cost homo-substrates and the wide use, by contrast, of sapphire and SiC, results in material with a high density of dislocations, typically 10^7–10^{10} dislocations cm^{-2}, depending on growth technique refinements.

In spite of this huge density of defects, the luminous efficiency of InGaN-based light emitting diodes (LEDs) is very high, a feature which has been assigned from the very beginning of nitride investigations to the existence in InGaN quantum wells (QWs) of localization centers acting as QDs and making them to a large extent insensitive to the high density of dislocations found in nitride material [1]. Although the nature of these localization centers is still an open question [2], their existence is undoubtedly crucial and has motivated the interest in *intentionally grown* GaN and InGaN QDs.

The most thermodynamically-stable crystallographic phase of nitride materials is the wurtzite one. This structure being non-centrosymmetric, a spontaneous polarization, oriented along the polar axis (c-axis), is present [3]. For polar heterostructures, the sheet charge densities created by the

 © 2008 IOP Publishing Ltd Printed in the UK

polarization discontinuities form a 'condenser-like' structure in which two charged planes face each other giving rise to a quasi-uniform electric field inside the confined structure. In the case of a lattice mismatch, a piezoelectric field is additionally present. As a whole, the combination of spontaneous and piezoelectric polarization results in a built-in electric field, in the MV cm^{-1} range. Consequently, optical properties of polar heterostructures are usually dominated by the quantum confined Stark effect resulting from the internal field [3]. The confined electrons and holes are spatially separated along the growth axis, leading to a red shift of the luminescence as well as to a reduced oscillator strength and eventually to a reduced radiative recombination rate which may turn out to be detrimental for LED applications [4].

The reduction/suppression of the built-in internal electric field which governs optical properties of polar heterostructures is the main motivation for growing and studying nonpolar heterostructures. In the peculiar case of nonpolar QWs for which the polarization is perpendicular to growth axis, the c axis does not cross any polarization discontinuity between the well and the barrier materials. As a consequence, there is no internal electric field in such QWs as was demonstrated in [5–7].

For nonpolar QDs, the situation is more complicated. Indeed, the c axis does cross GaN/AlN interfaces at two of the QD lateral facets so that a charge sheet density appears on these facets, possibly leading to an internal electric field inside the QD. However, the GaN/AlN spontaneous polarization difference being opposite to the piezoelectric one, contrary to the case of polar heterostructures, the internal electric field is expected to be strongly reduced in nonpolar QDs [8].

Restricted to the case of GaN, it is the aim of this review to address the issue of the growth of polar and nonpolar QDs. First, it will be shown that, depending on experimental parameters, the growth mode of GaN on AlN maybe of Frank–Van der Merwe or of Stranski–Krastanow type. In other words, the elastic strain stored when growing GaN on AlN may be relaxed either plastically by dislocation formation or elastically through 3D islanding.

Next, the structural properties of GaN QDs, the detailed knowledge of which is particularly crucial if we aim to calculate their optical properties, will be reviewed in detail. Optical properties of GaN QDs will be next presented. It is worth noting at this stage that due to the large bandgap discontinuity between AlN (about 6.2 eV) and GaN (about 3.47 eV), GaN QDs are particularly attractive for optical devices at high temperature. To illustrate the potential of these nanostructures, it should be recalled that triggered single-photon emission has been achieved from GaN QDs at 200 K [9], a much higher temperature than that required in quantum-information-processing schemes based on other III–V QDs which is easily reachable with thermo-electric cooling.

Last but not least, it will be shown that GaN QDs and AlN barriers do not exhibit significant interdiffusion, making GaN QDs a model system for studying growth and capping mechanisms, without facing the complications encountered when studying ternary InGaN QDs.

2. Epitaxial growth of nitrides

2.1. Generalities

The totality of commercial nitride-based LEDs is now produced using metalorganic chemical vapor deposition (MOCVD) technique. However, most of the results reviewed in the present paper refer to molecular beam epitaxy (MBE). The reason for that is familiar to growth physicists: MBE, being a low pressure technique, allows one to use reflection high energy electron diffraction (RHEED) in order to control *in situ* the growth process at a fraction of the monolayer scale. Such a tool is, of course, of particular interest for the growth of QDs and has also been extensively used for studying the specific GaN growth kinetics, as will be shown in section 2.2.

Although the situation is likely to change in the future due to the marked technological effort towards bulk GaN or AlN homo-substrates, sapphire or SiC substrates are the most commonly used. Until very recently, the lack of bulk nitride substrates, which has often been invoked as a serious limitation for the structural quality of the c-plane epilayers, was a particularly relevant issue for the case of the a-plane ones. To date, very few publications report the successful growth of bulk a-plane nitride layers exhibiting reasonably good structural quality. In a recent paper however, Paskova *et al* managed to grow low-defect-density homoepitaxial a-plane GaN on bulk a-plane GaN substrates, exhibiting a dislocation density in the 10^5 cm^{-2} range. These substrates, originating from Kyma technologies, were obtained by slicing a c-plane HVPE-grown GaN boule parallel to the $(11\bar{2}0)$ plane [10]. Nevertheless, this type of substrates, although already available to some extent, are not yet widely used by the GaN community, and the vast majority of groups are still using pseudosubstrates i.e. substrates with a nature different from that of the epitaxial layer, to perform growth.

Two types of pseudosubstrates are currently used for the heteroepitaxial growth of a-plane GaN or AlN layers: $(1\bar{1}02)$ r-plane sapphire [11–17] and $(11\bar{2}0)$ a-plane SiC [18–21]. This type of growth results in a high density of structural defects such as stacking faults ($\sim10^5$ cm^{-1}) and dislocations ($\sim10^9$ cm^{-2}) [10, 11, 21], an issue that has been partially solved by lateral epitaxial growth techniques employing SiO_2 stripe patterns [22]. To date, a-plane and m-plane GaN QDs have been achieved only on a-plane and m-plane SiC, this is why this review will be focused on the work carried out on this type of substrates.

2.2. GaN growth kinetics

As a matter of fact, nitride growth mechanisms are strongly dependent on experimental conditions, namely growth temperature and metal/nitrogen ratio value, leading to rough or smooth material surface, depending on adatom surface diffusion. As concerns the widely studied case of the c-plane, two different GaN growth regimes in MBE have been identified: the N-rich regime (with an excess of N with respect to Ga) and the Ga-rich regime (with an excess of Ga with respect to N) [23]. In the latter, an auto-surfactant effect of Ga (a segregation of Ga on the growing GaN surface leading to the

formation of a 2 monolayer (ML) thick Ga layer) has been put in evidence [24], and a coverage diagram, describing the Ga surface coverage during growth as a function of Ga flux and growth temperature, has been established [25] and is shown in figure 1(a).

Importantly, it has to be emphasized that the nature of the active N itself, i.e. ammonia or N plasma, drastically influences growth kinetics. Actually, the above considerations on the growth diagram, as well as most experimental results reported in this review, refer to plasma-assisted molecular beam epitaxy (PAMBE), active N being obtained by radio-frequency cracking of N_2 in a plasma cell.

It should be noted that the situation is different when active nitrogen results from cracking of ammonia. To our knowledge, no systematic study of Ga coverage has been performed in such a case but it is expected that adatom kinetics would be drastically influenced by residual H resulting from ammonia decomposition.

As concerns the a-plane, it has been found that growth also strongly depends on Ga/N flux ratio value. A growth diagram has been established and is shown in figure 1(b). Contrary to the case of c-plane GaN, no self-regulated Ga coverage has been found in this case but three regimes can be identified, namely a N-rich one, a regime characterized by a dynamical Ga coverage between 0 and 1 ML and, finally, a regime corresponding to Ga droplet accumulation. More precisely, it has been found that GaN growth in Ga-rich conditions results in a rough surface whereas growth in N-rich conditions leads to a smooth surface [26]. It is worth emphasizing that this situation is opposite to what is observed for polar nitrides. It suggests that surface diffusion barriers are lower in N-rich conditions than in Ga-rich conditions for $(11\bar{2}0)$ GaN, which again is the opposite of what is theoretically predicted [27] and experimentally observed [28] in the case of (0001) GaN growth.

As will be developed later, these kinetic considerations play a major role in the case of heterostructure growth, which may be of the Stranski–Krastanow (SK) or Frank–Van der Merwe (F-VdM) type, allowing one to grow either GaN QDs or quantum wells (QWs) depending on the value of the Ga/N ratio [29, 30].

When using the SK growth mode, self-organized GaN QDs have been obtained by taking advantage of the compressive strain experienced by GaN deposited on AlN or AlGaN, which is elastically relaxed through 3D islanding. As will be shown further in this review, the compressive strain by itself is insufficient and has to be combined with proper kinetic conditions. In other words, GaN QDs growth by PAMBE is performed in conditions leading to rough homoepitaxially grown material, as described in section 2.1, i.e. N-rich in the case of c-plane GaN QDs and Ga-rich in the case of a-plane and m-plane GaN QDs. Typical conditions leading, for T_s in the range from 740 to 750 °C, to growth of QDs or QWs for the heteroepitaxy of GaN on AlN are shown in figure 1.

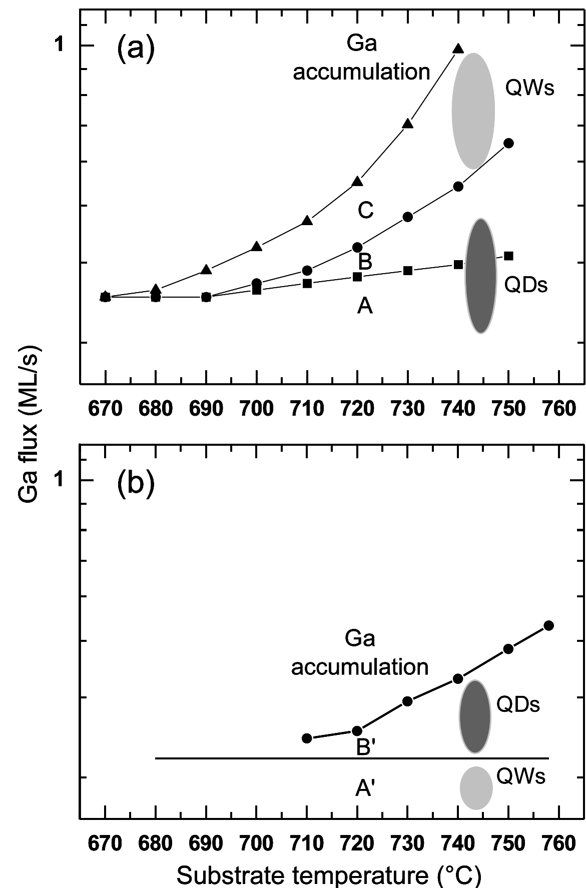

Figure 1. Ga flux dependence of the growth diagram for homoepitaxy of GaN, as a function of substrate temperature. (a) For [0001] GaN. The N flux is 0.35 ML s^{-1}. Four regions are identified: A: nitrogen-rich regime; B: dynamically-stable Ga coverage between 0 and 1 ML; C: self-regulated Ga bilayer regime; Ga accumulation regime (b) for $[11\bar{2}0]$ GaN. The N flux is 0.28 ML s^{-1}. three regions are identified: A′: nitrogen-rich regime; B′: dynamically-stable Ga coverage between 0 and 1 ML; Ga accumulation regime. The frontier line between A′ and B′ corresponds to the GaN growth rate at about 730 °C Typical conditions for growing QDs or QWs at $T_s = 745$ °C in the case of heteroepitaxy of GaN on AlN are indicated.

3. Growth of GaN QDs

Gallium nitride self-assembled quantum dots were grown for the first time by Tanaka and co-workers [31, 32] via low pressure metalorganic chemical vapor deposition (MOCVD). Si atoms were spread over the AlGaN surface leading to a SiN_x nanomasking of the surface and to formation of GaN QDs, approximately 20 nm in lateral size and 5 nm in height. The growth mode was likely of the Volmer–Weber type, with the absence of a wetting layer. A modification of Tanaka's antisurfactant method [31] has been recently proposed by Pakula *et al* [33, 34], consisting of producing a roughness in the AlGaN surface by means of a continuous flow of silane at very high temperatures, which led to a reduced dot density. Also using the MOCVD technique, Miyamura *et al* [35] obtained GaN/AlN QDs in the Stranski–Krastanow (SK) mode. An AlN layer of approx 100 nm was grown on a (0001)-oriented 6H-SiC substrate at elevated temperatures. The temperature was slightly reduced to grow GaN QDs. The diameter and height of the QDs are of the order of 20 and 2 nm, respectively, and the density could be varied between 10^9 and 10^{10} cm^{-2}. The size of the QDs was controlled to some extent by changing the growth temperature and V/III ratio during growth.

As concerns the MBE technique, it was demonstrated in 1997 by Daudin and co-workers that GaN dots can also be grown by PAMBE in the SK mode, starting from an AlN buffer layer [36]. Beyond a critical thickness of about 2.5 MLs, the initial bidimensional (2D) growth of GaN on AlN buffer layer on sapphire was followed by 3D islanding. After the formation of the dots, their capping by AlN led to recovery of a smooth AlN surface, allowing one to repeat the operation. Several stacks of quantum dots were actually grown with an AlN spacer of a few nanometers [37]. It was shown that below a given spacer thickness there is a vertical correlation mechanism [38], which will be described extensively in section 4. Along the views developed in section 2.2, it was further shown that GaN growth in Ga-rich conditions was of the F-VdM type, with elastic strain relaxation eventually occurring through dislocation formation rather than by 3D islanding. However, growth interruption followed by evaporation of Ga film in excess led to an instability of the 2D layer and to a spontaneous rearrangement of GaN into QDs. A better control of the dot density was achieved by using this so-called *modified*-SK growth mode [30].

Using ammonia-MBE, GaN/AlN QDs have also been fabricated on a Si(111) substrate [39]. A fully relaxed AlN layer was first grown. Interestingly, growth without interruption was found to lead to GaN plastic strain relaxation, starting at a thickness of approximately 3 nm, without 3D islanding. Introducing a growth interruption, an elastic strain relaxation was observed, resulting from the formation of 3D islands. The interruption had to be performed for a GaN thickness greater than 3 ML, which may be interpreted as a critical thickness for SK mode. The dot density is around 3×10^{11} cm^{-2} and the lateral and vertical size around 5 and 20 nm, respectively, similar to what is obtained in the case of PAMBE.

To conclude this section, it has to be stressed that GaN growth in ammonia-MBE is phenomenologically similar to GaN growth in PAMBE, when a Ga self-regulated bilayer is present. In both cases, growth occurs according to the F-VdM mode and growth interruption is necessary to induce 3D island formation, as an illustration that Ga bilayer on one hand, and H or N–H radicals adsorbed on the GaN surface on the other hand, can change the surface energy, eventually making free-surface formation energetically unfavorable with respect to dislocation formation.

3.1. Structural properties of GaN QDs

3.1.1. c-plane GaN QDs. Figure 2 shows a high resolution transmission electron microscopy (HRTEM) image of *c*-plane GaN QDs embedded in AlN. Based on a combination of HRTEM, AFM and reflection high energy electron diffraction (RHEED), the 3D shape of such QDs, namely an hexagonal truncated pyramid, has been determined and is shown as an inset in figure 2 [37]. At this stage, it is worth stressing that the wurtzite symmetry of nitrides is non-centrosymmetric. As a consequence the atomic stacking is not symmetric along some crystallographic directions, for instance along

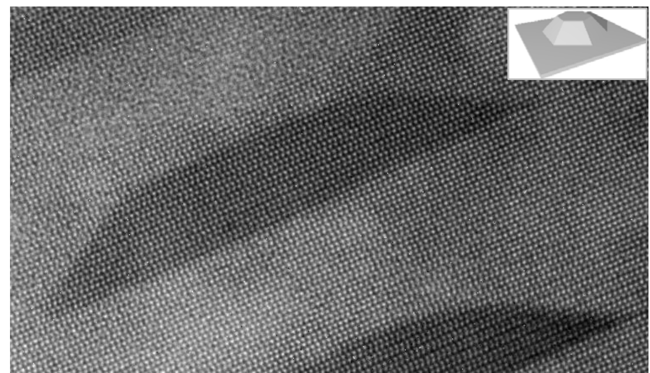

Figure 2. HRTEM image of GaN QDs embedded in AlN (JEOL 400 kV, courtesy of Dr J L Rouvière).

[0001], resulting in a charge separation which may lead to the existence of an electric field. This is particularly important for III-nitride semiconductors where the internal electric field is large [40] and where epitaxial layers are generally grown along the polar direction [0001]. Different tools have been used to determine the polarity of layers and surfaces, i.e. to discriminate between $+c$ and $-c$. Surface termination-sensitive chemical etching [41], high energy ion channeling [42], hemispherically scanned x-ray photoelectron diffraction [41] and convergent beam electron diffraction [43] (CBED) have been used. Recently, using HRTEM in the Z-contrast imaging mode with a probe-Cs-corrector, the local lattice polarity in AlN has been determined directly without any image simulation, by contrast to what is necessary when using CBED technique [44].

Using Z-contrast imaging, it is possible, as illustrated in figure 3, to establish that the polarity of [0001] GaN QDs is the same as that of surrounding AlN matrix., i.e $+c$ in the case under consideration [45].

However, it should be mentioned that $-c$ polarity GaN QDs have been grown on $-c$ polarity AlN deposited on C-terminated SiC [46]. The formation phenomenology of $-c$ polarity GaN QDs according to the SK growth mode as well as their structural and optical properties have been found to be similar to those of their $+c$ polarity counterpart.

3.1.2. a-plane GaN QDs. Growth of *a*-plane GaN QDs has been performed, using the growth conditions mentioned in section 2.2. As illustrated in figure 4, an alignment of the dots in rows along $[1\bar{1}00]$ is observed, which has been assigned to the anisotropic morphology of the *a*-plane AlN buffer layer [20].

Morphology of *a*-plane GaN QDs in $(11\bar{2}0)$ plane is markedly anisotropic [47]. Figure 5 shows HRTEM images of a stacking of *a*-plane GaN QDs. Viewed along the [0001] zone axis, they appear symmetric (see figure 4(a)) whereas a view along $[1\bar{1}00]$ reveals a shape asymmetry which has been correlated to the polarity of the *c*-axis. As shown in figure 5, the low angle facet of dots corresponds to the $+c$ direction.

3.1.3. m-plane GaN QDs. *m*-plane GaN QDs have been grown in a Ga-rich regime on an *m*-plane AlN buffer layer

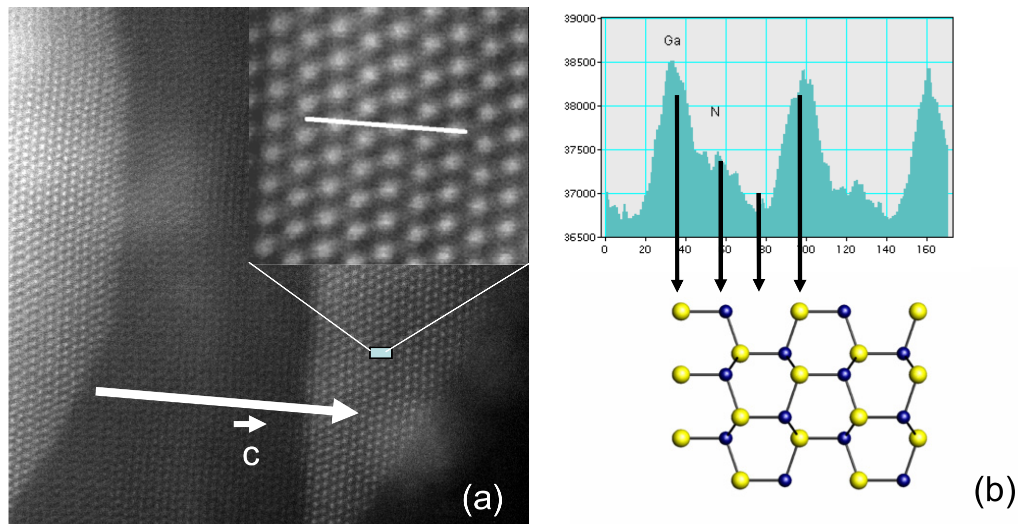

Figure 3. Polarity determination of c-plane GaN QDs embedded in c-plane AlN. (a) High resolution Z-contrast scanning transmission electron microscopy image. Inset: enlargement allowing one to identify Z-contrasted atomic columns. (b) Intensity profile along the white line in the inset and its assignment to asymmetrically stacked atomic columns along the c-direction.

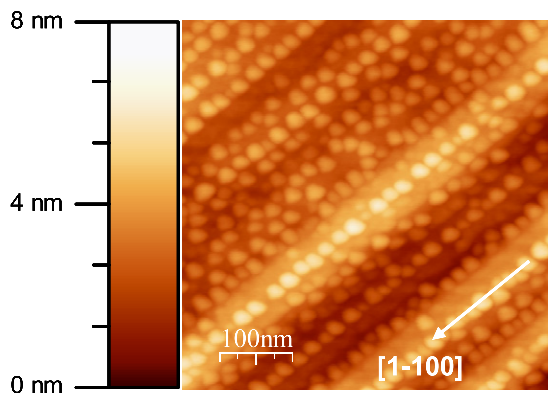

Figure 4. (1×1) μm^2 AFM micrographs of a-plane GaN QDs at the surface of a-plane AlN grown on a-plane SiC.

grown on an m-plane SiC. It has been seen that, depending on the strain state of the AlN buffer layer, GaN could relax its elastic energy by forming either QDs or QWires [48, 49]. This is illustrated in figure 6. It was found that a relaxed AlN buffer on SiC led to the formation of QDs whereas an unrelaxed AlN buffer layer exhibited an anisotropic strain state leading to the formation of QWires.

However, it was further established that even in the case of a relaxed AlN buffer favorable to the formation of QDs, increasing the amount of GaN deposited led to a shape transition from QDs to QWires. Such a behavior, restricted for GaN nanostructures to the case of m-plane orientation, has been observed in other material families and is consistent with theoretical predictions by Tersoff and Tromp, who have established that a transition shape from dot to wire may be observed as a function of the amount of material deposited [50]. In the present case, such a morphology transition is made possible by easy adatom diffusion along $[11\bar{2}0]$ in the $(1\bar{1}00)$ plane [51].

HRTEM analysis of m-plane GaN QDs and QWires has been performed [48]. As shown in figure 7, both nanostructures present a similar aspect when viewed along the $[11\bar{2}0]$ zone axis. As illustrated in figure 8, their asymmetric shape has been correlated to the polar orientation of the c-axis, the low angle facet corresponding to the $+c$ direction and the high angle facet to the $-c$ direction [45]. Then the shape asymmetry has been assigned to faster growth along the $+c$ direction than along $-c$.

The strain state of nanostructures similar to those shown in figures 6 and 7 has been studied by a combination of grazing incidence x-ray diffraction, diffraction absorption fine structure (DAFS) and HRTEM [49]. It has been found that $[1\bar{1}00]$ GaN QDs and QWires exhibit an asymmetric strain state, being markedly more relaxed along the c-axis than along $[11\bar{2}0]$. The large density of stacking faults in the c-plane has been identified as providing an efficient mechanism for easy elastic strain relaxation along the c-direction through the formation of partial dislocation terminating stacking faults at the AlN/GaN interface. Figure 9 is a HRTEM image of m-plane GaN QDs viewed along the $[11\bar{2}0]$ zone axis, with the presence of misfit dislocations at GaN/AlN interface.

4. Capping and vertical correlation of GaN QDs

4.1. Capping phenomenology

It has been found that capping of [0001] GaN QDs by AlN is associated to a homogeneous decrease in size of about one monolayer (see figure 10), on both the upper (0001) and the inclined $(1\bar{1}03)$ facets. Interestingly, this size reduction is not due to dot-barrier interdiffusion but most likely results from vertical exchange between Ga and Al, due to the higher stability of AlN at temperatures used for QD growth [52].

Next, following an initial wetting of dots with AlN up to 4 ML, further AlN growth proceeds in between dots up to 14 MLs which corresponds to AlN smoothing, according to

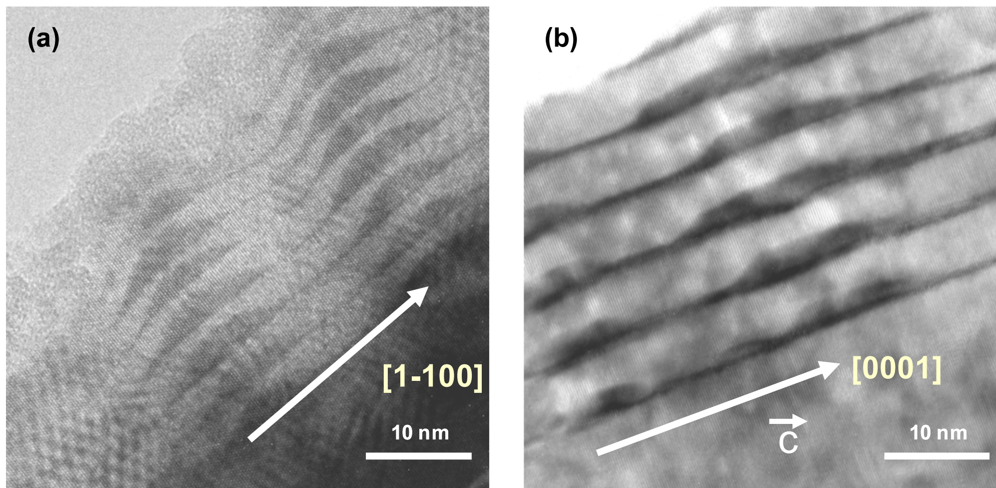

Figure 5. HRTEM images of a-plane GaN QDs viewed: (a) along the [0001] zone axis and (b) along the [$1\bar{1}00$] zone axis. The asymmetry of the dots is correlated to a c-direction polarity, as indicated (reproduced from [47], copyright 2007 American Institute of Physics).

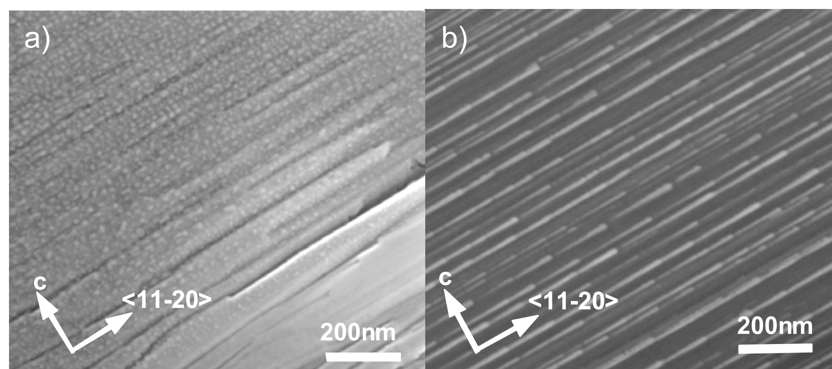

Figure 6. (a) GaN m-plane QDs and (b) QWires (after [49]).

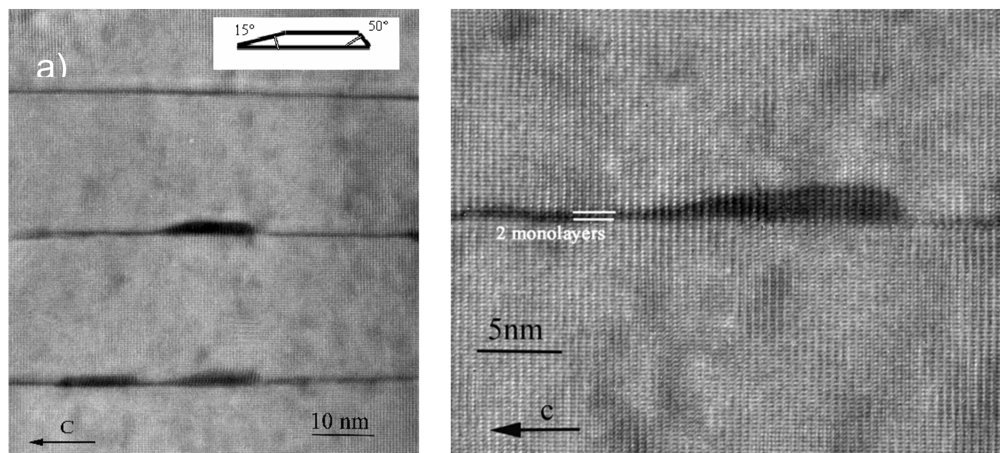

Figure 7. GaN m-plane nanostructures viewed along the [$11\bar{2}0$] zone axis: (a) QWires (b) QDs. The wetting layer, 2MLs thick is visible. Note the direction of the polar c-axis (reproduced from [48], copyright 2007 American Institute of Physics).

the schematic picture shown in figure 11 [53]. No change in dot shape and no noticeable interdiffusion are associated with capping.

As a consequence of capping, the strain state of GaN QDs changes as a function of AlN thickness. This evolution has been studied by a combination of x-ray techniques (multiwavelength anomalous diffraction and diffraction anomalous fine structure) using grazing incidence geometry and Raman spectroscopy. Actually, it is possible to probe selectively the phonon modes of QDs of various

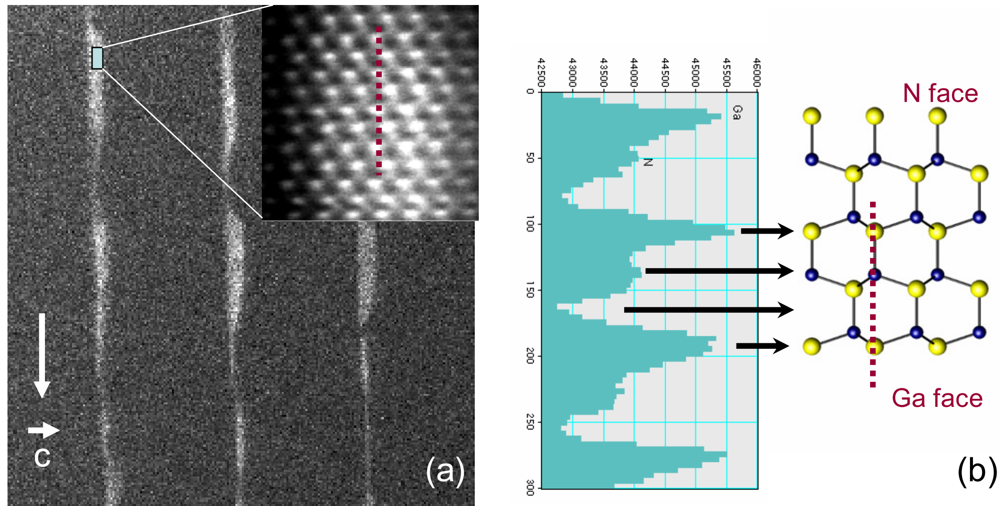

Figure 8. Determination of the c-axis polarity for m-plane GaN QDs embedded in an m-plane AlN. (a) High resolution Z-contrast scanning transmission electron microscopy image. Inset: enlargement allowing one to identify Z-contrasted atomic columns. (b) Intensity profile along the dotted line in the inset and its assignment to asymmetrically stacked atomic columns along the c-direction.

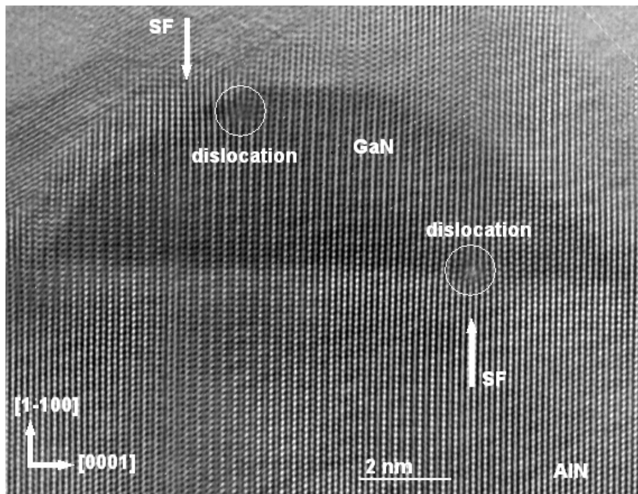

Figure 9. HRTEM image of m-plane GaN QDs viewed along the [11$\bar{2}$0] zone axis, with the presence of misfit partial dislocations at the GaN/AlN interface, associated to stacking faults (after [49]).

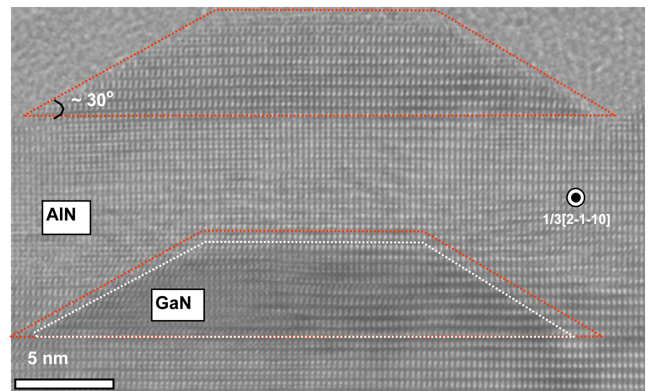

Figure 10. HRTEM image of [0001] GaN QDs on the surface and embedded in AlN. The embedded dot has lost about 1 ML following its capping by AlN (reproduced from [52], copyright 2004 American Institute of Physics).

sizes in single layers of GaN QDs by means of Raman scattering at various excitation energies in the UV [54]. By taking advantage of the resonance enhancement of the Raman signal, Cros *et al* [55, 56] have quantitatively studied the variation of ε_{xx} and ε_{zz} strain components in only one layer of GaN/AlN quantum dots as a function of AlN coverage. The QDs studied in this work were grown on 6H-SiC. The thickness of the AlN capping layer was varied from sample to sample, ranging from 0 to 14 ML. The resonance energy of the QDs was investigated by excitation with various UV laser lines. The comparison of the lattice parameters obtained by x-rays (triangles) and resonant Raman scattering (dots) as a function of coverage is shown in figure 12 [55]. It can be seen from the figure that the in-plane compression and axial expansion increase monotonically with capping thickness. It was found that the values of the in-plane lattice parameter obtained by both methods compares very well over the whole range of AlN capping investigated, in spite of the use of the biaxial approximation for the interpretation of the Raman data. Regarding the c parameter, the agreement was found to be good for small coverage (less than 4 ML). For thicker coverage the interpretation of the Raman results by means of the biaxial approximation underestimates the value of c by 0.4 %.

4.2. Vertical correlation of stacked QDs

The elastic interaction between GaN QDs and AlN barriers has been studied by electron microscopy [57, 58], x-rays diffraction [59, 60], Raman spectroscopy [61, 62] and theoretically [4, 62, 63].

As shown in figure 13, the elastic interaction between dots and barrier strongly depends on AlN spacer thickness, d, as shown by the corresponding Raman shift of AlN and GaN peaks: as seen by comparison to the position of the two arrows indicating the position of relaxed GaN and AlN in the bottom

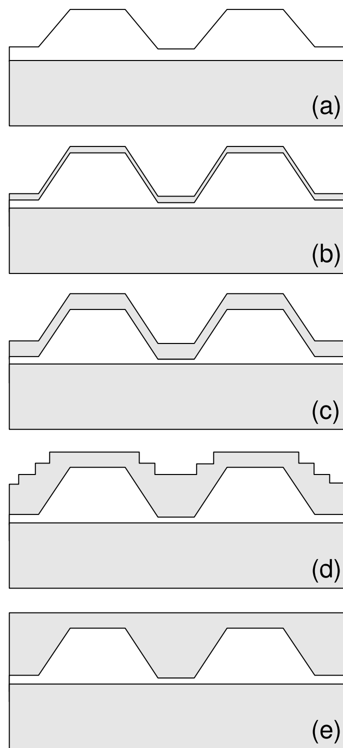

Figure 11. Schematic view of *c*-plane GaN dot capping by AlN. (a)–(c). Wetting of GaN by AlN up to 4 MLs coverage. (d)–(e) further growth of AlN in between dots until smoothing (reproduced from [53], copyright 2006 the American Physical Society).

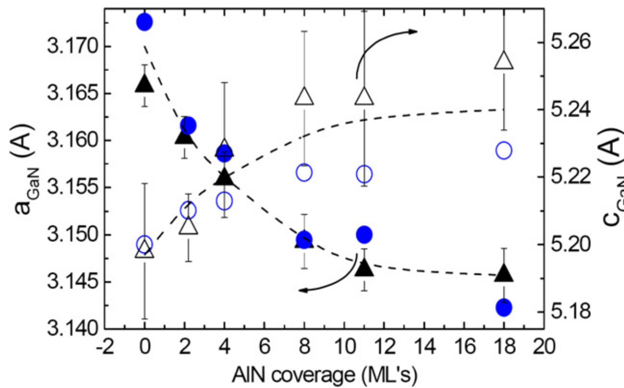

Figure 12. Comparison of a and c lattice parameters of GaN QDs obtained by x-ray measurements (triangles) and micro-Raman scattering (dots). The dashed lines are guides to the eyes (reproduced from [55], copyright 2008 Wiley).

part of the figure, it is concluded that the thinner the barrier, the more relaxed the dots and the more strained the barrier whereas, conversely, the thicker the barrier, the more strained the dots and the more relaxed the barrier.

An advantage has been taken of these features to study the vertical correlation of stacked GaN QD planes, as illustrated in figure 14 in the case of *c*-plane GaN dots grown by PAMBE.

It has been found that vertical correlation results in an increase of the lateral size of the dots with increased number of layers and a decreasing of the density with the number of

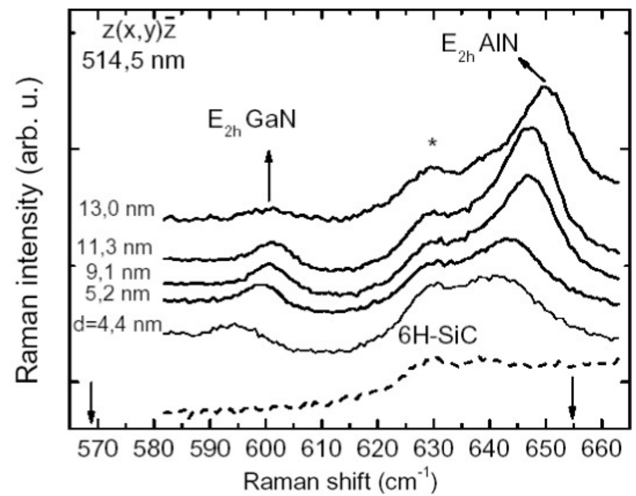

Figure 13. Raman shift of E2h GaN and AlN modes as a function of AlN spacer thickness, d. Note the arrow in lower left (respectively lower right) showing the position of relaxed GaN (respectively AlN) (reproduced from [61], copyright 2006 Wiley).

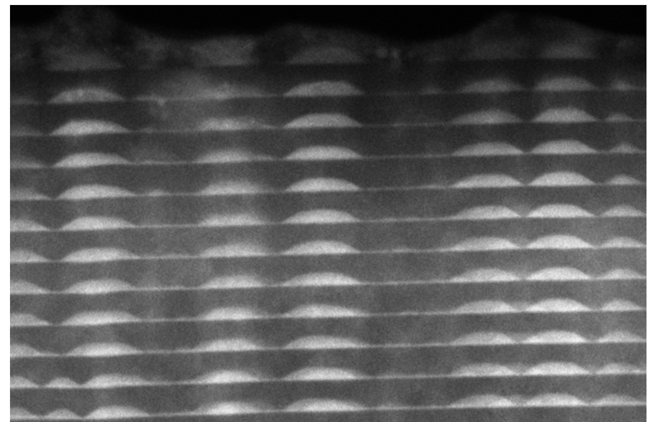

Figure 14. High resolution Z-contrast scanning transmission electron microscopy image of stacked *c*-plane GaN QDs (courtesy of Dr J L Rouvière).

periods [64]. A vertical correlation has also been observed in the case of dots grown by MOCVD [65]. As expected, the vertical correlation depends on the thickness of the AlN spacer. As a matter of fact, correlation effects were found for an AlN spacer thickness as large as 8 nm [64], no correlation was found for an AlN spacer thickness of 20 nm [36]. In the case of (MOCVD dots) [65], the AlN spacer separating the dot layers was of 20 nm. The observed vertical correlation, in apparent contradiction with the results of [64], has been assigned to the fact that MOCVD dots [65] are three times larger in diameter as compared to the dots of [64].

It should be mentioned at this stage that the key phenomena associated with vertical correlation of GaN dots, i.e. their volume increase and density decrease, are similar to what has been observed in other semiconductor families, namely in the case of InAs and SiGe QDs. However, a remarkable specificity of the GaN/AlN system is the absence of interdiffusion which makes it a model one to study the barrier/dot elastic interplay.

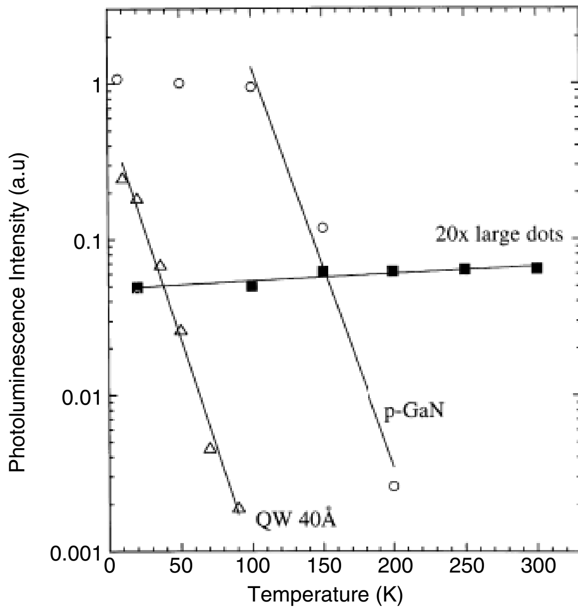

Figure 15. Comparison of PL intensity of p-GaN, GaN quantum well and a stack of 20 planes of GaN QDs as a function of temperature (reproduced from [68], copyright 1999 Elsevier).

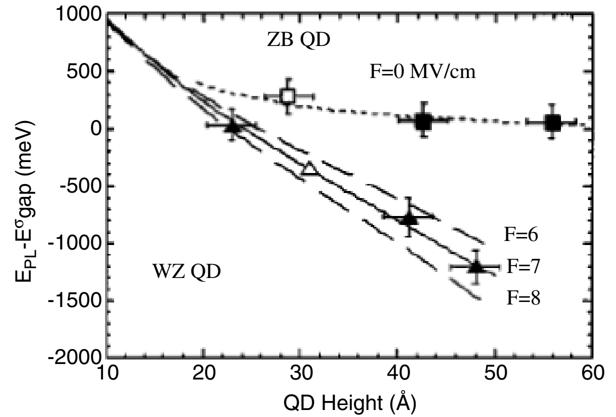

Figure 16. Energy shift of QD emission with respect to the GaN bandgap energy as a function of the QD height. ZB QD refers to cubic phase [001] GaN QDs, with no electric field. WZ QD refers to the wurtzite phase *c*-plane GaN QDs. For a height of about 2.5 nm, emission is observed at the GaN gap (reproduced from [70], copyright 2003 the American Physical Society).

5. Optical properties

5.1. Emission of an ensemble of GaN QDs

5.1.1. c-plane QDs. As recalled above, optical properties of polar heterostructures are usually dominated by the quantum confined Stark effect resulting from the internal field [3]. As a consequence of spatial separation of confined electrons and holes along the growth axis, the photoluminescence spectrum of GaN QDs is observed to be red-shifted below the bulk GaN bandgap energy for a dot height larger than about 2.5 nm [66]. As a further consequence, the reduction in spatial overlap of the electron and hole wavefunctions induced by the internal electric field has a dramatic effect on the radiative recombination rate [66, 67]. For three-dimensionally confined wavefunctions with negligible excitonic effect the radiative decay rate is proportional to the electron–hole wavefunction overlap. This leads to very long decay times ranging from 5 ns to 200 μs for polar GaN/AlN QDs with sizes ranging from 1.5 to 3.5 nm [67]. From these experimental results, it was deduced that the electric field can be as high as 9 MV cm^{-1} for the GaN/AlN system.

In the same way as in other self-assembled systems, GaN QDs also present a large inhomogeneity in QD sizes resulting in large inhomogeneous broadening. However, in GaN QDs embedded in AlN, it has been established that the effect of dot height distribution is amplified by the presence of an internal electric field, leading to photoluminescence (PL) peaks which are several hundreds of meV wide [37]. Nevertheless, the integrated intensity of the GaN QD PL is found to be constant from 4 K up to room temperature, as can be seen in figure 15, as carrier migration to nonradiative centers is hindered by strong confinement. By contrast, a marked quenching in the PL intensity of GaN bulk and quantum well systems is observed for increasing temperature, due to the high density of threading dislocations and other defects that act as nonradiative traps [68].

The strength of the built-in electric field in self-assembled GaN/AlN QDs has been estimated/calculated both experimentally and theoretically [67, 69–73]. The values exhibit a considerable dispersion, ranging from 3.8 to 9 MeV cm^{-1}. One possible reason for this dispersion can be attributed to the uncertainty in dot height determination by atomic force microscopy. In addition residual doping partially screening the electric field may be invoked. Furthermore, there is an ongoing controversy about the magnitude of the difference in the spontaneous polarization between AlN and GaN that may seriously affect the value of the internal fields [74, 75].

The variation of PL emission as a function of QD height is shown in figure 16. Remarkably, dots in the 4–5 nm height range exhibit a luminescence more than 1 eV *below* GaN gap [70], as a consequence of the quantum confined Stark effect (QCSE) induced by the internal electric field. It has been eventually shown that by tuning the height of GaN QDs embedded in AlN, PL can be varied between blue and orange [76].

Another case of the QCSE is observed when studying the dependence of the emission upon excitation power [69, 77, 78]. In this case an increasing blue shift of the emission energy is observed as a function of increasing excitation density, resulting from the partial screening of the internal electric field by the field induced by the photogenerated electron–hole dipoles.

In the case of a pulsed excitation, a strongly blue-shifted emission with respect to the low power continuous excitation regime is observed, followed by a progressive shift of the PL peak to the red as a function of the delay with respect to the pulse (see figure 17) [79]. This effect has been assigned to progressive recombination of photogenerated carriers associated to a recovery of the internal electric field.

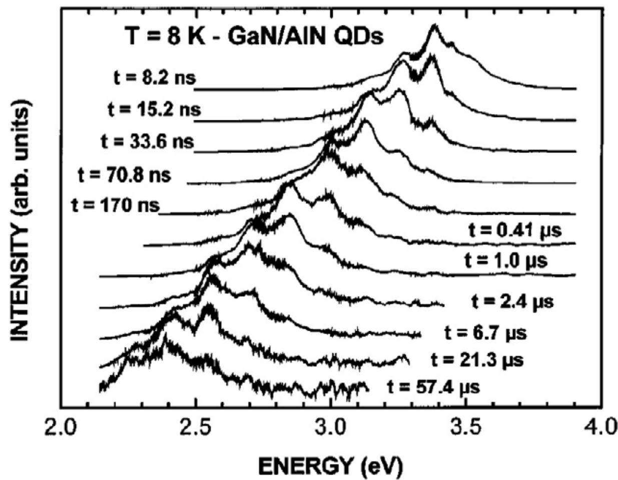

Figure 17. PL shift as a function of time delay after the excitation pulse. Reprinted with permission from [79]. Copyright 2003 by the American Physical Society.

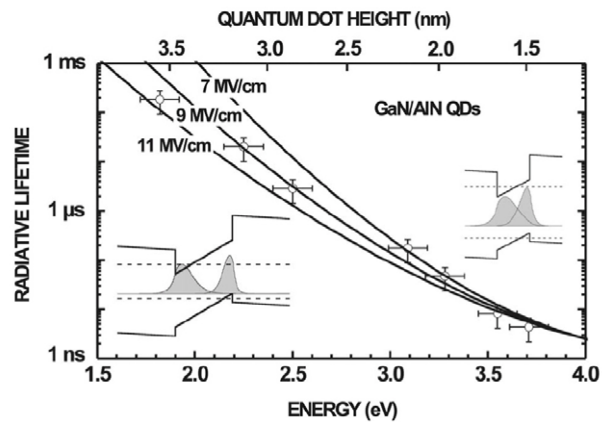

Figure 18. PL decay time as a function of the energy of the PL maximum /QD height for different GaN/AlN QDs. Inset: schematic representation of band diagram and electron and hole wavefunction overlap depending on the height of the dots. The upper right (respectively lower left) case corresponds to small (respectively big) dots. Reprinted with permission from [67]. Copyright 2006 by the American Physical Society.

It has been calculated that the blue shift of the emission energy with increasing electron–hole pair density should be linear [72]. It should be noted that cathodoluminescence experiments performed on GaN QDs have exhibited a blue shift of the luminescence peak with respect to photoluminescence. This has been assigned to the somewhat higher excitation density obtained in this technique, resulting in a larger screening of the electric field which may lead to a blue shift appreciably higher than in photoluminescence experiments [80, 81].

The spatial separation of electrons and holes inside GaN QDs reduces the overlap between the electron and hole wavefunctions and the magnitude of the exciton oscillator strength [73]. Hence, the presence of strong built-in electric fields should slow down the exciton radiative recombination. Consistent with this statement, time-resolved PL experiments have revealed that the decay time of the emission, τ_D, can be as long as tens of microseconds and presents a strong dependence on the QD height [67, 70, 79, 82], as shown in figure 18. Such a variation of τ_D is characteristic of the QCSE, with lower emission energies correspond to higher QDs where the separation of electrons and holes is more pronounced and τ_D is longer, whereas for smaller dots the emission energy is higher, with a higher overlap between the electron and hole wavefunctions leading to shorter τ_D. A simple theoretical model, based on the effective mass and envelope function approximations, that assumes a constant effective electric field inside the QD was used to analyze the results and is shown as solid lines in figure 18 [67].

To conclude this section, it should be mentioned at this stage that the functioning of GaN QDs by doping with rare earth ions has been examined, in view of visible light emission applications. The idea of combining the RE luminescence with a semiconductor host arose from using Er and Yb (infrared) in GaAs, GaP, Si and SiC. In particular Er doped Si structures have been well investigated since the research was driven by the appeal of integration with Si microelectronics. For intense and thermally-stable visible light emission from electroluminescence devices, wide bandgap semiconductors are required since efficient energy transfers can only occur if the bandgap of the host is wider than the energy difference between RE^{3+} ground states and excited state. The choice of GaN as a semiconductor host is particularly appropriate because of its direct bandgap, required for a good semiconductor host-RE^{3+} ion energy transfer probability and because it is a III–V semiconductor so that RE ions occupy metal sites with 3+ charge. Actually, it has been shown that the carrier confinement properties of GaN QDs could be successfully associated to the RE^{3+} visible light emission properties, i.e. red (Eu), blue (Tm) or green (Tb). Consistently, almost no quenching of luminescence was observed up to room temperature, as an evidence of an efficient energy transfer to RE^{3+} ions [83–86].

5.1.2. a-plane and m-plane QDs. The recent interest in nonpolar QDs, namely *a*-plane [47] and *m*-plane [48] is motivated by the expectation of a reduced internal electric field and an increased radiative recombination efficiency. However, the overall optical properties of nonpolar QDs are not obvious to forecast. Indeed, in that case, the polar axis (*c* axis) is in the plane of the layers. In the case of nonpolar quantum wells, the situation is quite simple: the polar axis is parallel to the GaN/AlN interfaces. There is thus no discontinuity of the polarization perpendicular to the interfaces so that there is no internal electric field. In spite of exhibiting a wurtzite structure, a nonpolar quantum well thus behaves like a 'standard' quantum well for which only confinement effects are present. As concerns *a*-plane quantum wells, this was confirmed experimentally in several publications [87, 88].

The situation is indeed more complicated in the case of nonpolar QDs as the polarization vector does have a component along the normal to the quantum dot lateral facets. Therefore a sheet charge density due to this polarization charge density appears on the QDs lateral facets. This charge density is thus likely to generate an internal electric field that will induce a quantum confined Stark effect. The geometry of the

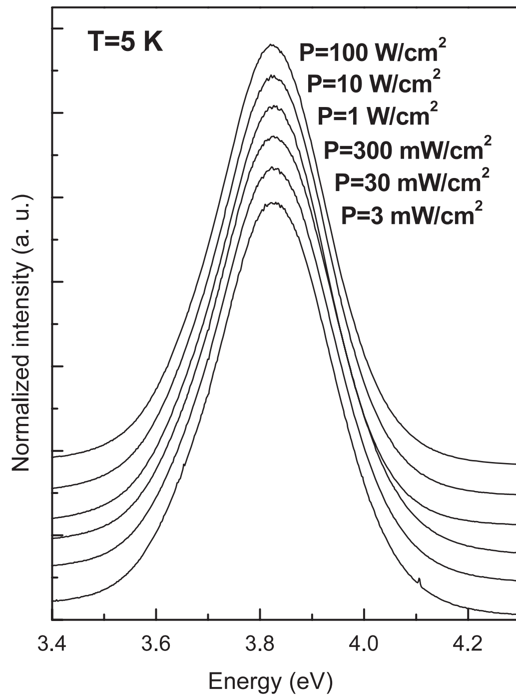

Figure 19. Photoluminescence spectrum at 5 K for various excitation power densities (at $\lambda = 244$ nm). The luminescence is above the GaN bandgap, and no screening effect is observed in this excitation power range (reproduced from [90], copyright 2005 American Institute of Physics).

situation is however very different from the situation of polar QDs and QWs.

For polar heterostructures, the sheet charge densities created by the polarization discontinuities form a 'condenser-like' structure in which two charged planes face each other giving rise to a quasi-uniform electric field inside the confined structure (even for quantum dots). For nonpolar quantum dots, the geometry is quite different because only the two side facets of the QDs that are crossed by the c-axis carry a charge [89]. This is thus a three-dimensional electrostatic problem, and the precise determination of the internal electric field requires a knowledge of the dot geometry, the strain distribution and the residual doping of the samples. Concerning this last issue, it can be shown that each lateral facet of a nonpolar dot carries the equivalent of between one and two elementary charges, so that the presence of a few electrons in each dot can drastically screen the internal electric field.

A photoluminescence experiment on an ensemble of a-plane GaN QDs, as a function of excitation power density is shown in figure 19. Clearly, the photoluminescence occurs above the GaN bandgap, so that the confinement effects dominate over the quantum confined Stark effect [90]. This is markedly different from the case of polar quantum dots of similar sizes described in section 5.1.1, for which the quantum confined Stark effect leads to a spectacular red shift of the luminescence of the QDs. Moreover, there is no indication of screening over the range of excitation densities that was probed. Again this is unlike polar GaN QDs for which the screening of the internal field by the photogenerated carriers is observable over a wide excitation density range, as evoked in section 5.1.1.

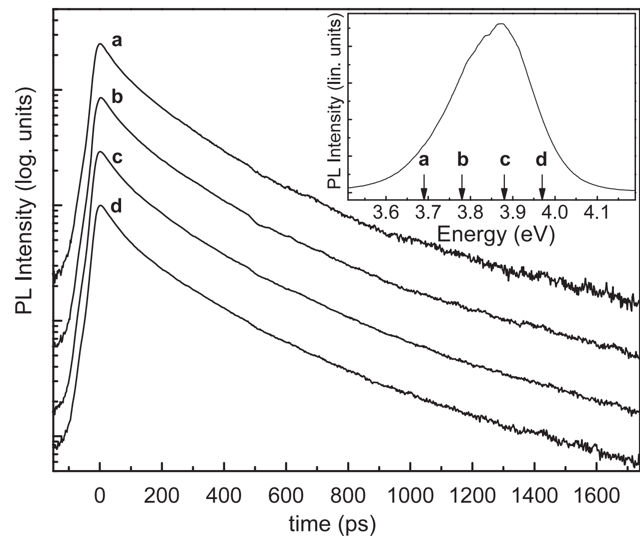

Figure 20. Time-resolved photoluminescence at various emission wavelengths. The decay curves are independent of emission wavelength (reproduced from [91], copyright 2007 American Physical Society).

As previously shown, the radiative lifetime of the confined excitons is very sensitive to the spatial separation of electrons and holes induced by the QCSE. This is especially true for nonpolar structures as the two charged planes are spatially well separated (by one QD diameter): in that case even a small internal electric field will separate the electron and hole wavefunctions and thus drastically reduce the transition oscillator strength, while the energy of the transition would be little affected.

Experiments of time-resolved PL are shown in figure 20. The first striking feature is the fact that the photoluminescence decay curves are independent of the emission energy [91]. This means that the oscillator strength does not depend on the QD size. This differs appreciably from the behavior of polar QDs, for which the oscillator strength decreases exponentially with QD size [66, 67]. The second striking feature in the photoluminescence decay curves is that the decay is very fast as compared to the decay of polar GaN QDs (see section 5.1.1). Although the decay is not monoexponential, an average decay time of around 280 ps can be extracted. This is to be compared with lifetimes ranging between a few ns and several 100s μs for polar QDs [66, 67].

These experiments, in particular the fact that the radiative decay curves do not depend at all on QD size, are experimental evidence that no effect of an internal electric field on the optical properties of an ensemble of nonpolar QDs can be supported. This conclusion also holds for m-plane GaN QDs which have been recently grown [48]. Also for these dots, PL has been observed above the energy of GaN bandgap and the PL decay time was found to be in the range of 250 ps, as a clue that QCSE does not affect the optical properties of these nanostructures.

5.2. *Emission of polar single QDs*

The large inhomogeneous broadening of the spectral lines in the case of an assembly of QDs makes impossible the detailed study of the exciton fine structure, the homogeneous

broadening of the emission lines and other fundamental properties of the emission process. Such information is accessible by performing single dot spectroscopy, a task particularly delicate in the case of GaN QDs due to the high dot density generally obtained, related to the high density of defect-related nucleation centers [92] (see section 3).

MicroPL experiments have been reported on single GaN QDs grown by MOCVD [93] as well as cathodoluminescence of uncapped GaN dots grown on AlGaN [94]. In both cases, the density of dots was small enough to make experiments possible without using specific isolation techniques. Alternatively, microPL was achieved on processed samples obtained by etching submicron mesa patterns [94] or opening submicron holes in an opaque metallic mask [95] on a sample containing a low density of QDs ($<10^{10}$ cm^{-2}).

For low excitation powers, authors of [93] have observed a single emission peak which has been attributed to the confined exciton. With increasing power, a second peak, attributed to the biexciton, appears on the high energy side. The identification of both peaks was supported by the fact that the intensity varied linearly and quadratically, respectively, with excitation power. According to this assignment, the biexciton binding energy was found to be negative and of the order of 30 meV. This feature, namely negative binding energies observed in GaN QDs, is a consequence of the spatial separation of electrons and holes which simultaneously leads to a reduction of the electron–hole binding energy and to an increase of the electron–electron and hole–hole binding energies [96].

Remarkably, it was recently shown that binding energy could actually be tuned from negative, for high dots, to positive, for smaller ones, directly related to the dominant effect of QCSE for large dots [97]. This effect is specific to nitrides. In addition, in the case of small dots where the effect of QCSE can be neglected, a decrease of the exciton binding energy was found for increasing lateral confinement, an effect usually observed in InAs/GaAs QDs [98].

Although the line width of the exciton peak can be as small as 700 μeV [97], this is still considerably wider that usually observed in InAs QDs. Such a large inhomogeneous broadening has been assigned to spectral diffusion, i.e. fluctuations in the exciton energy produced by the variations in the strength of the internal field caused by charge fluctuations in the vicinity of the QDs [99, 100]. This effect has been experimentally quantified by measuring the time evolution of the continuous wave microPL spectrum of single GaN QDs over a long timescale [95], allowing one to identify two types of spectral diffusion: a discrete one where the emission peak jumps abruptly in an energy range of the order of 10 meV, and a continuous shift of the transitions producing an inhomogeneous broadening of the spectral lines. Both effects were assigned to charges trapped in the vicinity of dots, either close, allowing one to observe a discrete energy jump, or at a longer distance, giving rise to a continuous shift [95].

5.3. Emission of nonpolar single QDs

The microPL of single *a*-plane GaN QDs has been performed on small mesas allowing one to isolate a few tens of dots [91].

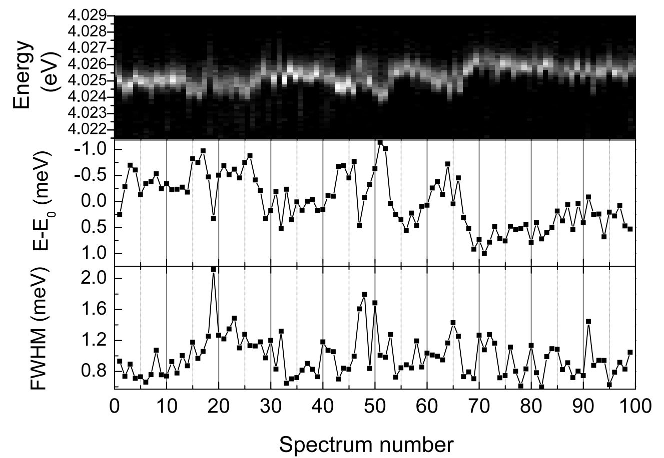

Figure 21. Energy position and full width at half maximum of a single dot emission. Each spectrum is integrated over one second (reproduced from [91], copyright 2007 the American Physical Society).

Single lines were better isolated on the high energy side of the QD distribution due to the lower spectral density of QD emission. It was checked that their intensity varied linearly with excitation power at low power, consistent with their assignment to the recombination of a single electron–hole pair and not to excited states recombination.

The measured linewidths of single dot lines ranged from 0.5 to 2 meV. Similar to the case of polar QDs examined in section 5.2, this broadening was attributed to spectral diffusion [99, 100], i.e. loosely bound charges around a given dot are trapped and detrapped as a function of time, leading to a time-dependent potential variation in the quantum dot that shifts the discrete transitions of the QD.

This phenomenon can actually be observed on the typical integration time (1 s) used in these experiments, as shown in figure 21. Both discrete changes in peak position and in linewidth were observed as a function of time, consistent with the presence of mobile charges trapped in the vicinity of dots. It is worth noting that the linewidth is smaller than for polar QDs, where it can be as wide as 20 meV [93]. It has to be pointed out that spectral diffusion depends to a large extent on the sample quality and excitation conditions. However, the relatively small linewidths observed for nonpolar QDs are consistent with the fact that the internal field—which enhances spectral diffusion—is much lower in nonpolar QDs. As a consequence of these relatively narrow linewidths, the study of single dot PL lines as a function of temperature was made possible, revealing a temperature-dependent broadening which is shown in figure 22. This broadening of the line at high temperature is characteristic of coupling to acoustic phonons [91].

It has been shown that the lineshape becomes asymmetric when raising the temperature, which is characteristic of the appearance of acoustic phonon emission and absorption events [101–104]. When increasing the temperature, the acoustic phonon population builds up, thus increasing the probability of absorbing or emitting acoustic phonons when an electron–hole pair radiatively recombines. The asymmetry

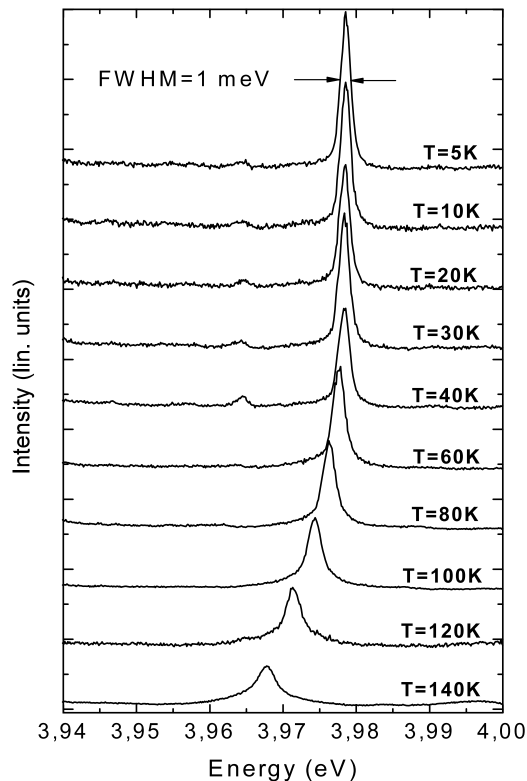

Figure 22. Evolution of the emission lineshape of a single QD (reproduced from [91], copyright 2007 the American Physical Society).

of the line, more marked on the red side, results from the fact that emission events are more probable than absorption events. The experimental observation of this coupling to acoustic phonons allows one to probe the spatial extent of the confined wavefunctions [101]. The detailed analysis has been performed in [91] and led to the conclusion that the full width at half maximum extent for the center of mass is $2\xi = 4.2$ nm. The key point is that this value is much smaller than the typical quantum dot diameter, as an indication that a supplemental localization inside the quantum dots occurs.

Such an hypothesis is further supported by time-resolved experiments on single PL lines. Contrary to the case of a collection of dots examined in section 5.1.2, the decay time of each line was found to be monoexponential. Surprisingly, it was found in addition that different single dots lines exhibited different decay times, with no apparent correlation to emission energy. This feature supports the interpretation that the decay time is dominated by the localization length inside the QD, and not by the actual QD size [91].

6. Conclusion

As a conclusion, it appears that GaN presents unique characteristics, compared to QD-forming materials pertaining to other semiconductor families. The ability of GaN to form polar and nonpolar QDs, the presence of a huge electric field in polar QDs, the lack of interdiffusion between dots and barrier, including during the capping process make this system rather unique. Optical properties of polar dots are dominated by the quantum confined Stark effect. By contrast, no effect assigned to the presence of an electric field has been observed in the case of nonpolar ones. However, in both cases, an in depth understanding of optical properties is far from being reached, due to a lack of control of residual doping level in both dots and barriers. Detailed optical studies on single *a*-plane GaN QDs have shown a reduced spectral diffusion compared to the case of polar dots, consistent with the reduction in internal electric field intensity. Analyzing the temperature dependence of the PL linewidth of *a*-plane QDs led to the conclusion that excitons are laterally localized at a length scale smaller than the dot size. Furthermore, no direct correlation was found between monoexponential decay time constants and dot size. Thus it can be concluded that the localization of the exciton itself does not simply depend on dot size, making the nature of localization in these nonpolar QDs an issue which still remains open.

Although this review was limited to GaN QDs, we hope that we have made clear that the concept of QDs, principally of InGaN QDs, has been associated from the very beginning of the research of nitrides. On the one hand, the exact nature of localization centers behaving as QDs in the InGaN active region of GaN-based light emitting diodes is as far from the scope of the present review as the issue of InGaN QDs themselves, so that neither have been evoked. On the other hand, the concept of QDs behaving as perfect crystallographic nano-objects embedded in a defective matrix is certainly of general interest as cheap, abundant and reliable homo-substrates are not available. In view of this, we believe that polar and nonpolar GaN QDs may be used in the future as the active region of UV LEDs. In addition, the large energy bandgap difference between AlN and GaN makes GaN QDs promising candidates for room temperature optoelectrical applications such as single-photon emission. Finally, it was also one aim of this review to show that the GaN/AlN system, being free of interdiffusion, may be considered as a model system to study basic properties of QDs.

Acknowledgments

Helpful discussions with Dr B Gayral are gratefully acknowledged, as well as continuous interaction with colleagues and students from CEA Grenoble. Drs J L Rouvière and C Bougerol are especially acknowledged for the content of figures 3 and 8.

References

[1] Nakamura S 1998 *Science* **281** 957
[2] See for instance the papers in the Oliver R and Daubin B (ed) 2007 *Phil. Mag.* 87 p 1967 (Special Issue)
[3] Bernardini F, Fiorentini V and Vanderbilt D 1997 *Phys. Rev.* B **56** R10024
[4] Andreev A D and O'Reilly E P 2000 *Phys. Rev.* B **62** 15851
[5] Waltereit P, Brandt O, Trampert A, Grahn H T, Menniger J, Ramsteiner M, Reiche M and Ploog K H 2000 *Nature* **406** 865
[6] Craven M D, Waltereit P, Speck J S and DenBaars S P 2004 *Appl. Phys. Lett.* **84** 496
[7] Akopian N, Bahir G, Gershoni D, Craven M D, Speck J S and DenBaars S P 2005 *Appl. Phys. Lett.* **86** 202104

[8] Cros A, Budagosky J A, García-Cristóbal A, Garro N, Cantarero A, Founta S, Mariette H and Daudin B 2006 *Phys. Status Solidi* b **243** 1499

[9] Kako S, Santori C, Hoshino K, Gotzinger S, Yamamoto Y and Arakawa Y 2006 *Nat. Mater.* **5** 887

[10] Paskova T, Kroeger R, Figge S, Hommel D, Darakchieva V, Monemar B, Preble E, Hanser A, Williams N M and Tutor M 2006 *Appl. Phys. Lett.* **89** 051914

[11] Craven M D, Lim S H, Wu F, Speck J S and DenBaars S P 2002 *Appl. Phys. Lett.* **81** 469

[12] Ng H M 2002 *Appl. Phys. Lett.* **80** 4369

[13] Chen C, Yang J, Wang H, Zhang J, Adivarahan V, Gaevski M, Kuokstis E, Gong Z, Su M and Asif Khan M 2003 *Japan. J. Appl. Phys.* **42** L640

[14] Paskov P P, Schifano R, Monemar B, Paskova T, Figge S and Hommel D 2005 *J. Appl. Phys.* **98** 093519

[15] Kusakabe K and Ohkawa K 2005 *Japan. J. Appl. Phys.* **44** 7931

[16] Tsuchiya Y, Okadome Y, Honshio A, Miyake Y, Kawashima T, Iwaya M, Kamiyama S, Amano H and Akasaki I 2005 *Japan. J. Appl. Phys.* **44** L1516

[17] Chevtchenko S, Ni X, Fan Q, Baski A A and Morkoç H 2006 *Appl. Phys. Lett.* **88** 122104

[18] Onojima N, Suda J, Kimoto T and Matsunami H 2003 *Appl. Phys. Lett.* **83** 5208

[19] Craven M D, Wu F, Chakraborty A, Imer B, Mishra U K, DenBaars S P and Speck J S 2004 *Appl. Phys. Lett.* **84** 1281

[20] Founta S, Rol F, Bellet-Amalric E, Bleuse J, Daudin B, Gayral B, Moisson C and Mariette H 2005 *Appl. Phys. Lett.* **86** 171901

[21] Zakharov D N, Liliental-Weber Z, Wagner B, Reitmeier Z J, Preble E A and Davis R F 2005 *Phys. Rev.* B **71** 235334

[22] Craven M D, Lim S H, Wu F, Speck J S and DenBaars S P 2002 *Appl. Phys. Lett.* **81** 1201

[23] Tarsa E J, Heying B, Wu X H, Fini P, DenBaars S P and Speck J S 1997 *J. Appl. Phys.* **82** 5472

[24] Mula G, Adelmann C, Moehl S, Oullier J and Daudin B 2001 *Phys. Rev.* B **64** 195406

[25] Adelmann C, Brault J, Jalabert D, Gentile P, Mariette H, Mula G and Daudin B 2002 *J. Appl. Phys.* **91** 9638

[26] Koblmüller G, Wu F, Mates T, Speck J S, Fernandez-Garrido S and Calleja E 2007 *Appl. Phys. Lett.* **91** 221905

[27] Neugebauer J, Zywietz T K, Scheffler M, Northrup J E, Chen H and Feenstra R M 2003 *Phys. Rev. Lett.* **90** 056101

[28] Daudin B, Feuillet G, Mula G, Mariette H, Rouvière J L, Pelekanos N, Fishman G, Adelmann C and Simon J 1999 *Phys. Status Solidi* a **176** 621

[29] Adelmann C, Gogneau N, Sarigiannidou E, Rouvière J L and Daudin B 2002 *Appl. Phys. Lett.* **81** 3064

[30] Gogneau N, Jalabert D, Monroy E, Shibata T, Tanaka M and Daudin B 2003 *J. Appl. Phys.* **94** 2254

[31] Tanaka S, Iwai S and Aoyagi Y 1996 *Appl. Phys. Lett.* **69** 4096

[32] Tanaka S, Ramvall P, Nomura S, Hirayama H and Aoyagi Y 1998 *Electron. Commun. Japan* I **81** 20

[33] Pakuła K, Bożek R, Surowiecka K, Stępniewski R, Wysmolek A and Baranowski J M 2006 *Phys. Status Solidi* b **243** 1486

[34] Pakuła K, Bożek R, Surowiecka K, Stępniewski R, Wysmolek A and Baranowski J M 2006 *J. Cryst. Growth* **289** 472

[35] Miyamura M, Tachibana K, Someya T and Arakawa Y 2002 *J. Cryst. Growth* **237/239** 1316

[36] Daudin B, Widmann F, Feuillet G, Samson Y, Arlery M and Rouvière J L 1997 *Phys. Rev.* B **56** R7069

[37] Widmann F, Daudin B, Feuillet G, Samson Y, Rouvière J L and Pelekanos N 1998 *J. Appl. Phys.* **83** 7618

[38] Coraux J, Renevier H, Favre-Nicolin V, Renaud G and Daudin B 2006 *Appl. Phys. Lett.* **88** 153125

[39] Damilano B, Grandjean N, Semond F, Massies J and Leroux M 1999 *Phys. Status Solidi* b **216** 451

[40] Bernardini F and Fiorentini V 1998 *Phys. Rev.* B **57** R9427

[41] Rouviere J L, Weyher J L, Seelmann-Eggebert M and Porowski S 1998 *Appl. Phys. Lett.* **73** 668

[42] Daudin B, Rouviere J L and Arlery M 1996 *Appl. Phys. Lett.* **69** 2480

[43] Rouviere J L, Arlery M, Neibuhr R, Bachem K H and Briot O 1996 *MRS Internet J. Nitride Semicond. Res.* **1** 33

[44] Mkhoyan K A, Batson P E, Cha J, Schaff W J and Silcox J 2006 *Science* **312** 1354

[45] Rouvière J L, Bougerol C, Amstatt B, Bellet-Amalric E and Daudin B 2008 *Appl. Phys. Lett.* **92** 201904

[46] Monroy E, Sarigiannidou E, Fossard F, Gogneau N, Bellet-Amalric E, Mank H and Daudin B 2004 *Appl. Phys. Lett.* **84** 3684

[47] Founta S, Bougerol C, Vennegues P, Mariette H and Daudin B 2007 *J. Appl. Phys.* **102** 074304

[48] Amstatt B, Renard J, Bougerol C, Bellet-Amalric E, Gayral B and Daudin B 2007 *J. Appl. Phys.* **102** 074913

[49] Amstatt B, Landré O, Favre-Nicolin V, Proietti M G, Bellet-Amalric E, Bougerol C, Renevier H and Daudin B 2008 *J. Appl. Phys.* at press

[50] Tersoff J and Tromp R M 1993 *Phys. Rev. Lett.* **70** 2782

[51] Amstatt B, Bougerol C, Rouvière J L, Bellet-Amalric E and Daudin B 2008 *Phys. Rev.* B submitted

[52] Gogneau N, Jalabert D, Monroy E, Sarigiannidou E, Rouvière J L, Shibata T, Tanaka M, Gerard J M and Daudin B 2004 *J. Appl. Phys.* **96** 1104

[53] Coraux J, Amstatt B, Budagoski J A, Bellet-Amalric E, Rouvière J-L, Favre-Nicolin V, Proietti M G, Renevier H and Daudin B 2006 *Phys. Rev.* B **74** 195302

[54] Kuball M, Gleize J, Tanaka S and Aoyagi Yoshinobu 2001 *Appl. Phys. Lett.* **78** 987

[55] Cros A, Budagosky J A, Garro N, Cantarero A, Coraux J, Renevier H, Proietti M G, Favre-Nicolin V and Daudin B 2007 *Phys. Status Solidi* c **4** 2379

[56] Cros A, Garro N, Cantarero A, Coraux J, Renevier H and Daudin B 2007 *Phys. Rev.* B **76** 165403

[57] Arlery M, Rouvière J L, Widmann F, Daudin B, Feuillet G and Mariette M 1999 *Appl. Phys. Lett.* **74** 3287

[58] Sarigiannidou E, Andreev A D, Monroy E, Daudin B and Rouvière J L 2005 *Appl. Phys. Lett.* **87** 203112

[59] Chamard V, Metzger T H, Bellet-Amalric E, Daudin B, Adelmann C, Mariette H and Mula G 2001 *Appl. Phys. Lett.* **79** 1971

[60] Chamard V, Metzger T H, Sztucki M, Holý V, Tolan M, Bellet-Amalric E, Adelmann C, Daudin B and Mariette H 2003 *Europhys. Lett.* **63** 268

[61] Fresneda J *et al* 2007 *Phys. Status Solidi* c **4** 2342

[62] Cros A, Garro N, Llorens J M, García-Cristóbal A, Cantarero A, Gogneau N, Monroy E and Daudin B 2006 *Phys. Rev.* B **73** 115313

[63] Williams D P, Andreev A D, O'Reilly E P and Faux D A 2005 *Phys. Rev.* B **72** 235318

[64] Gogneau N, Fossard F, Monroy E, Monnoye S, Mank H and Daudin B 2004 *Appl. Phys. Lett.* **84** 4224

[65] Hoshino K, Kako S and Arakawa Y 2004 *Appl. Phys. Lett.* **85** 1262

[66] Simon J, Pelekanos N T, Adelmann C, Martinez-Guerrero E, André R, Daudin B, Dang L S and Mariette H 2003 *Phys. Rev.* B **68** 035312

[67] Bretagnon T, Lefebvre P, Valvin P, Bardoux R, Guillet T, Taliercio T, Gil B, Grandjean N, Semond F, Damilano B, Dussaigne A and Massies J 2006 *Phys. Rev.* B **73** 113304

[68] Widmann F, Simon J, Pelekanos N T, Daudin B, Feuillet G, Rouvière J L and Fishman G 1999 *Microelectron. J.* **30** 353

[69] Widmann F, Simon J, Daudin B, Feuillet G, Rouvière J L and Pelekanos N T 1998 *Phys. Rev.* B **58** R15989
[70] Simon J, Pelekanos N T, Adelmann C, Martínez-Guerrero E, André R, Daudin B, Dang L S and Mariette H 2003 *Phys. Rev.* B **68** 035312
[71] Nakaoka T, Kako S and Arakawa Y 2006 *Phys. Rev.* B **73** 121305
[72] Ranjan V, Allan G, Priester C and Delerue C 2003 *Phys. Rev.* B **68** 115305
[73] Andreev A D and O'Reilly E P 2000 *Phys. Rev.* B **62** 15851
[74] Bernardini F, Fiorentini V and Vanderbilt D 1997 *Phys. Rev.* B **56** R10024
[75] Hogg R A, Norman C E, Shields A J, Pepper M and Iizuka M 2000 *Appl. Phys. Lett.* **76** 1428
[76] Damilano B, Grandjean N, Semond F, Massies J and Leroux M 1999 *Phys. Status Solidi* b **216** 451
[77] Riblet P, Tanaka S, Ramvall P, Nomura S and Aoyagi Y 1999 *Solid State Commun.* **109** 377
[78] Kalliakos S, Bretagnon T, Lefebvre P, Taliercio T, Gil B, Grandjean N, Damilano B, Dussaigne A and Massies J 2004 *J. Appl. Phys.* **96** 180
[79] Bretagnon T, Kalliakos S, Lefebvre P, Valvin P, Gil B, Grandjean N, Dussaigne A, Damilano B and Massies J 2003 *Phys. Rev.* B **68** 205301
[80] Salviati G, Martinez O, Mazzoni M, Rossi F, Armani N, Gucciardi P, Vinattieri A, Alderighi D, Colocci M, Gonzalez M A, Sanz-Santacruz L F and Massies J 2002 *J. Phys.: Condens. Matter* **14** 13329
[81] Salviati G, Rossi F, Armani N, Grillo V, Martinez O, Vinattieri A, Damilano B, Matsuse A and Grandjean N 2004 *J. Phys.: Condens. Matter* **16** S115
[82] Kako S, Miyamura M, Tachibana K, Hoshino K and Arakawa Y 2003 *Appl. Phys. Lett.* **83** 984
[83] Hori Y, Jalabert D, Andreev T, Monroy E, Tanaka M, Oda O and Daudin B 2004 *Appl. Phys. Lett.* **84** 2247
[84] Andreev T, Hori Y, Biquard X, Monroy E, Jalabert D, Farchi A, Tanaka M, Oda O, Dang L S and Daudin B 2005 *Phys. Rev.* B **71** 115310
[85] Andreev T, Liem N Q, Hori Y, Tanaka M, Oda O, Dang L S and Daudin B 2006 *Phys. Rev.* B **73** 195203
[86] Andreev T, Liem N Q, Hori Y, Tanaka M, Oda O, Dang L S, Daudin B and Gayral B 2006 *Phys. Rev.* B **74** 155310
[87] Waltereit P, Brandt O, Trampert A, Grahn H T, Menniger J, Ramsteiner M, Reiche M and Ploog K H 2000 *Nature* **406** 865
[88] Akopian N, Bahir G, Gershoni D, Craven M D, Speck J S and DenBaars S P 2005 *Appl. Phys. Lett.* **86** 202104
[89] Cros A, Budagosky J A, García-Cristóbal A, Garro N, Cantarero A, Founta S, Mariette H and Daudin B 2006 *Phys. Status Solidi* b **243** 1499
[90] Garro N, Cros A, Budagosky J A, Cantarero A, Vinattieri A, Gurioli M, Founta S, Mariette H and Daudin B 2005 *Appl. Phys. Lett.* **87** 011101
[91] Rol F, Founta S, Mariette H, Daudin B, Dang Le Si, Bleuse J, Peyrade D, Gérard J M and Gayral B 2007 *Phys. Rev.* B **75** 125306
[92] Rouvière J L, Simon J, Pelekanos N, Daudin B and Feuillet G 1999 *Appl. Phys. Lett.* **75** 2632
[93] Kako S, Hoshino K, Iwamoto S, Ishida S and Arakawa Y 2004 *Appl. Phys. Lett.* **85** 64
[94] Petersson A, Gustafsson A, Samuelson L, Tanaka S and Aoyagi Y 1999 *Appl. Phys. Lett.* **74** 3513
[95] Bardoux R, Guillet T, Lefebvre P, Taliercio T, Bretagnon T, Rousset S, Gil B and Semond F 2006 *Phys. Rev.* B **74** 195319
[96] Williams D P, Andreev A D, Faux D A and O'Reilly E P 2004 *Physica* E **21** 358
[97] Simeonov D, Dussaigne A, Butté R and Grandjean N 2008 *Phys. Rev.* B **77** 075306
[98] Rodt S, Heitz R, Schliwa A, Sellin R L, Guffarth F and Bimberg D 2003 *Phys. Rev.* B **68** 035331
[99] Rice J H, Robinson J W, Jarjour A, Taylor R A, Oliver R A, Briggs G A D, Kappers M J and Humphreys C J 2004 *Appl. Phys. Lett.* **84** 4110
[100] Moriwaki O, Someya T, Tachibana K, Ishida S and Arakawa Y 2000 *Appl. Phys. Lett.* **76** 2361
[101] Besombes L, Kheng K, Marsal L and Mariette H 2001 *Phys. Rev.* B **63** 155307
[102] Bayer M and Forchel A 2002 *Phys. Rev.* B **65** 041308
[103] Favero I, Cassabois G, Ferreira R, Darson D, Voisin C, Tignon J, Delalande C, Bastard G, Roussignol P and Gérard J M 2003 *Phys. Rev.* B **68** 233301
[104] Peter E, Hours J, Senellart P, Vasanelli A, Cavanna A, Bloch J and Gérard J M 2004 *Phys. Rev.* B **69** 041307